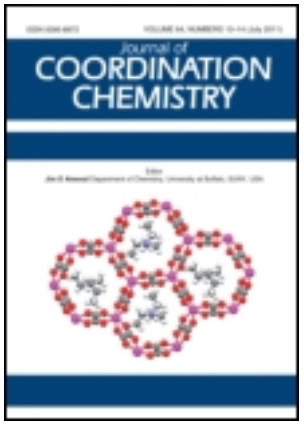

Journal of Coordination Chemistry
Publication details, including instructions for authors and subscription information:
http://www.tandfonline.com/loi/gcoo20

Hg^{II}-containing MOFs constructed from bis-benzimidazole-based ligand with highly selective anion-exchange capacity

Bo Xiao [a] , Li-Jun Yang [b] , Hai-Yang Xiao [b] & Shao-Ming Fang [b]

[a] Nanjing University of Information Science & Technology , Jiangsu Key Laboratory of Atmospheric Environment Monitoring and Pollution Control , School of Environmental Science and Engineering, Nanjing 210044 , Jiangsu , PR China

[b] Henan Provincial Key Laboratory of Surface and Interface Science , Zhengzhou University of Light Industry , Zhengzhou , Henan 450002 , PR China

Published online: 02 Dec 2011.

To cite this article: Bo Xiao , Li-Jun Yang , Hai-Yang Xiao & Shao-Ming Fang (2011) Hg^{II}-containing MOFs constructed from bis-benzimidazole-based ligand with highly selective anion-exchange capacity, Journal of Coordination Chemistry, 64:24, 4408-4420, DOI: 10.1080/00958972.2011.639875

To link to this article: http://dx.doi.org/10.1080/00958972.2011.639875

Journal of Coordination Chemistry
Vol. 64, No. 24, 20 December 2011, 4408–4420

Hg^{II}-containing MOFs constructed from bis-benzimidazole-based ligand with highly selective anion-exchange capacity

BO XIAO*†, LI-JUN YANG‡, HAI-YANG XIAO‡ and SHAO-MING FANG*‡

†Nanjing University of Information Science & Technology, Jiangsu Key Laboratory of Atmospheric Environment Monitoring and Pollution Control, School of Environmental Science and Engineering, Nanjing 210044, Jiangsu, PR China
‡Henan Provincial Key Laboratory of Surface and Interface Science, Zhengzhou University of Light Industry, Zhengzhou, Henan 450002, PR China

(*Received 30 March 2011; in final form 31 October 2011*)

Two Hg(II)-containing metal–organic frameworks (MOFs) based on 1,1′-(1,5-pentanediyl)*bis*-1*H*-benzimidazole (pbbm), $\{[HgBr_2(pbbm)]\cdot DMF\}_n$ (**1**) and $[HgI_2(pbbm)]_2$ (**2**), have been constructed to explore new and potent ion-exchange materials. Single-crystal X-ray diffraction shows that **1** features a 1-D zigzag chain framework, while **2** presents a dimeric structure in which two Hg(II) cations are bridged by two pbbm ligands. The significant differences of these MOFs indicate that the counteranions have impact on assembling and structures of the resultant MOFs. Remarkably, coordinated Br^- in **1** can be replaced completely when the solid polymer is treated with an aqueous solution containing I^-. Confirmation of retention of structure is provided by FT-IR spectra and the XRPD pattern. The thermal stabilities of **1** and **2** have also been investigated.

Keywords: Hg^{II} complexes; Crystal structure; Coordinated anion exchange; Thermal stability

1. Introduction

Crystal engineering of metal–organic frameworks (MOFs) have applications in many areas, such as catalysis, sensing, magnetism, and ion exchange [1]. In such materials, functionality can be introduced from either the inorganic species or the organic building blocks. Furthermore, the combination produces cooperative effects so as to enhance the properties. However, rational control over topologies and optimized properties is a challenge due to labile coordination geometries of metal sites, versatile coordination modes of organic building blocks, and subtle factors from crystallization conditions such as counteranion, temperature, and solvent [2]. Especially, counteranion effects can be drastic since they exhibit coordination, and thus vary the conformation and even the assembly pattern of some MOFs, or in a template role, are involved in non-covalent

*Corresponding authors. Email: boxiao@zzuli.edu.cn; smfang@zzuli.edu.cn

ISSN 0095-8972 print/ISSN 1029-0389 online © 2011 Taylor & Francis
http://dx.doi.org/10.1080/00958972.2011.639875

interactions such as hydrogen-bonding or π–π stacking to stabilize the metal–organic assembly [3]. Therefore, research is indispensable to probe the influence of counteranion on the overall molecular architectures to extend knowledge of relevant structural types with the aim of rational control of MOFs.

As an important property of coordination frameworks, anion exchange has attracted attention because it makes such adducts potentially attractive as anion-exchange materials [4–6]. For example, coordination solids that preferentially sequester certain anions could be used to treat wastewater contaminated with negatively charged toxic or radioactive species [7]. In the cases reported, exchange generally occurs among guest anions. The weak interaction between these guest anions and the cationic framework results in a relatively easy exchange. Exchange of coordinated anions is more difficult than that of guest anions, as it involves both rupture of the old bond and formation of the new one. Some attempts to bring about coordinated anion exchange have proven unsuccessful [8, 9]. With this in mind, we synthesize two Hg^{II} complexes, $\{[HgBr_2(pbbm)]\cdot DMF\}_n$ (**1**) and $[HgI_2(pbbm)]_2$ (**2**), and discuss the influence of different counteranions on product formations as well as their anion-exchange behavior. Significantly, the framework of **1** can undergo facile anion exchange for I^- in the crystalline solid state at room temperature. This phenomenon is supported by IR spectra, X-ray powder diffraction (XRPD), scanning electron microscope (SEM), and energy-dispersive X-ray spectroscopy (EDS).

2. Experimental

2.1. *Materials and general methods*

With the exception of 1,1′-(1,5-pentanediyl)*bis*-1*H*-benzimidazole (pbbm), which was synthesized according to reported literature procedure [10], all of the starting materials and solvents were obtained commercially and used as received, or purified by standard methods prior to use. IR spectra were recorded from 4000 to 400 cm^{-1} on a Tensor 27 OPUS (Bruker) FT-IR spectrometer with KBr pellets. Elemental analyses were carried out by using a Flash EA 1112 analyzer. Thermogravimetric analysis (TGA) experiments were carried out on a Perkin-Elmer Diamond SII thermal analyzer from room temperature to 520°C under nitrogen at a heating rate of 10°C min^{-1}. The XRPD patterns were recorded on a Rigaku D/Max-2500 diffractometer, operated at 40 kV and 100 mA, using a Cu-target tube and a graphite monochromator. Intensity data were recorded by continuous scan in a $2\theta/\theta$ mode from 3° to 80° with a step size of 0.02° and a scan speed of 8° min^{-1}. SEM and EDS were recorded on a JSM-6490LV electron microscope.

2.2. *Synthesis of $\{[HgBr_2(pbbm)]\cdot DMF\}_n$ (1)*

A 5 mL solution of pbbm (60.8 mg, 0.2 mmol) in methanol was dropwise added to a 1 mL DMF solution of $HgBr_2$ (0.1 mmol) and then shaken to give a clear colorless solution. Slow evaporation of the solvent at room temperature gave colorless single crystals suitable for X-ray single-crystal analysis after 2 weeks. Crystals are stable in air and insoluble in common organic solvents. Yield: ~50% based on pbbm. Anal. Calcd

for $C_{22}H_{27}Br_2HgN_5O$ (%): C, 35.81; H, 3.69; N, 9.49. Found (%): C, 35.85; H, 3.67; N, 9.52. IR (ν, cm^{-1}): 3444m, 3089w, 2938m, 2885m, 1779w, 1669w, 1608m, 1459s, 1384m, 1244w, 1198m, 1137s, 934m, 750s, 634s, 495w, 423m.

2.3. *Synthesis of [HgI_2(pbbm)]$_2$ (2)*

A 6 mL methanol solution of pbbm (30.4 mg, 0.1 mmol) was layered carefully above a 4 mL DMF solution of HgI_2 (45.4 mg, 0.1 mmol) and then filtered to give a clear colorless solution. Slow evaporation of the solvent at room temperature gave colorless single crystals suitable for X-ray single-crystal analysis after 3 days. Yield: ~57% based on pbbm. Anal. Calcd for $C_{19}H_{20}HgI_2N_4$ (%): C, 30.07; H, 2.66; N, 7.38. Found (%): C, 30.11; H, 2.63; N, 7.41. IR (ν, cm^{-1}): 3423m, 3102w, 2938m, 2885m, 1762w, 1659w, 1614m, 1462s, 1393m, 1255w, 1205m, 1102s, 923m, 743s, 623s, 493w, 425m.

2.4. *X-ray structure analyses*

X-ray single-crystal diffraction measurements for **1** and **2** were carried out on a Bruker Smart 1000 CCD diffractometer equipped with a graphite crystal monochromator situated in the incident beam for data collection at 293(2) K. Determinations of unit cell parameters and data collections were performed with Mo-Kα radiation ($\lambda = 0.71073$ Å) and unit cell dimensions were obtained with least-square refinements. The program SAINT [11] was used for integration of the diffraction profiles. Semi-empirical absorption corrections were applied using SADABS [12]. The structure was solved by direct methods using the SHELXS program of the SHELXTL package and refined with SHELXL [13]. Metals in the complex were located from the E-maps, and other non-hydrogen atoms were located in successive difference Fourier syntheses and refined with anisotropic thermal parameters on $|F|^2$. Hydrogen atoms were added theoretically, riding on the concerned atoms and refined with fixed thermal factors. Further crystallographic data and experimental details for structural analyses are summarized in table 1. Selected bond lengths and angles are listed in table 2.

2.5. *Ion-exchange measurement*

Freshly prepared crystals of **1** and **2** were each immersed in a certain concentration aqueous solution of KX ($X = F, Cl, I$) at room temperature. The mixture was left for several days and the resulting products were filtered off, washed several times with water and methanol, and then dried in air. The products were characterized by IR absorption spectroscopy, SEM, EDS, and XRPD analysis.

3. Results and discussion

3.1. *Crystal structure of {[$HgBr_2$(pbbm)]·DMF}$_n$ (1)*

Single-crystal X-ray diffraction reveals that **1** crystallizes in the monoclinic space group *P2(1)/n*. As shown in figure 1(a), the geometry of Hg^{2+} is tetrahedral with two imidazole nitrogen atoms from individual pbbm ligands and two Br^- ions.

Table 1. Crystal data and details of measurements for **1** and **2**.

Complex	**1**	**2**
Empirical formula	$C_{22}H_{27}Br_2HgN_5O$	$C_{19}H_{20}HgI_2N_4$
Formula weight	758.78	737.90
Crystal system	Monoclinic	Monoclinic
Space group	*C2/c*	*P2(1)/n*
Unit cell dimensions (Å, °)		
a	19.471(2)	11.7831(8)
b	10.564(1)	14.4426(8)
c	21.295(3)	14.6872(10)
α	90.00	90.00
β	100.343(11)	94.730(6)
γ	90.00	90.00
Volume (Å^3), *Z*	4309.1 (9), 8	2490.9(3), 4
Calculated density (g cm^{-3})	2.339	1.968
μ (mm^{-1})	10.02	9.410
Reflections collected/unique	8677/4007	17,830/4627
R(int)	0.040	0.0385
Final R^a and wR^b	0.041 and 0.087	0.0262 and 0.0277

[a] $R = \Sigma(||F_o| - |F_c||)/\Sigma|F_o|$; [b] $wR = [\Sigma w(|F_o|^2 - |F_c|^2)^2/\Sigma w(|F_o|^2)^2]^{1/2}$.

Table 2. Selected bond lengths (Å) and angles (°) for **1** and **2**.

$\{[HgBr_2(pbbm)] \cdot DMF\}_n$ (**1**)			
Hg(1)–N(4)#1	2.271(3)	Hg(1)–Br(1)	2.5423(4)
Hg(1)–Br(2)	2.4989(4)	N(4)–Hg(1)#2	2.271(3)
Hg(1)–N(1)	2.318(3)		
N(4)#1–Hg(1)–N(1)	97.31(10)	N(4)#1–Hg(1)–Br(1)	105.65(8)
N(4)#1–Hg(1)–Br(2)	113.10(8)	N(1)–Hg(1)–Br(1)	100.56(8)
N(1)–Hg(1)–Br(2)	111.66(8)	Br(2)–Hg(1)–Br(1)	124.575(19)
$[HgI_2(pbbm)]_2$ (**2**)			
Hg1–N2	2.302(6)	Hg1–I2	2.7156(7)
Hg1–N4A#1	2.418(7)	Hg1–I1	2.6513(7)
N2–Hg1–N4A#1	92.7(2)	N2–Hg1–I2	102.48(16)
N2–Hg1–I1	115.86(15)	N4A#1–Hg1–I2	98.46(16)
N4A#1–Hg1–I1	108.34(17)	I1–Hg1–I2	131.12(2)

Symmetry codes: **1**: #1: $x+1/2$, $-y+3/2$, $z-1/2$; #2: $x-1/2$, $-y+3/2$, $z+1/2$. **2**: #1: $-x+1/2$, $-y+3/2$, $-z+1$.

The deviation from a tetrahedron is probably caused by the preference of Hg^{2+} for soft donor bromides [14]. This distortion leads to a significant difference between two Hg–N bond lengths (2.318(3) and 2.271(3) Å). Hg–Br bond lengths (2.5423(4) and 2.4989(4) Å) are normal compared to other Hg^{2+} systems [14]. The N–Hg–Br bond angles range from 105.65(8)° to 113.10(8)°. Larger bond angles of Br–Hg–Br (124.575(19)°) and smaller N–Hg–N angles (97.31(10)°) in the polymer are consistent with the preference of Hg^{2+} for Br^-. The solid state structure of $[HgBr_2(pbbm)]_n$ is similar to that of the piperazine–pyridine adduct [15]. The polymeric chains extend along the *a*-direction through $HgBr_2$ units bridged by pbbm. The tetrahedral coordination geometry around Hg^{2+} is beneficial for the formation of a zigzag polymeric structure, and the distance between Hg^{2+} ions is 11.638 Å.

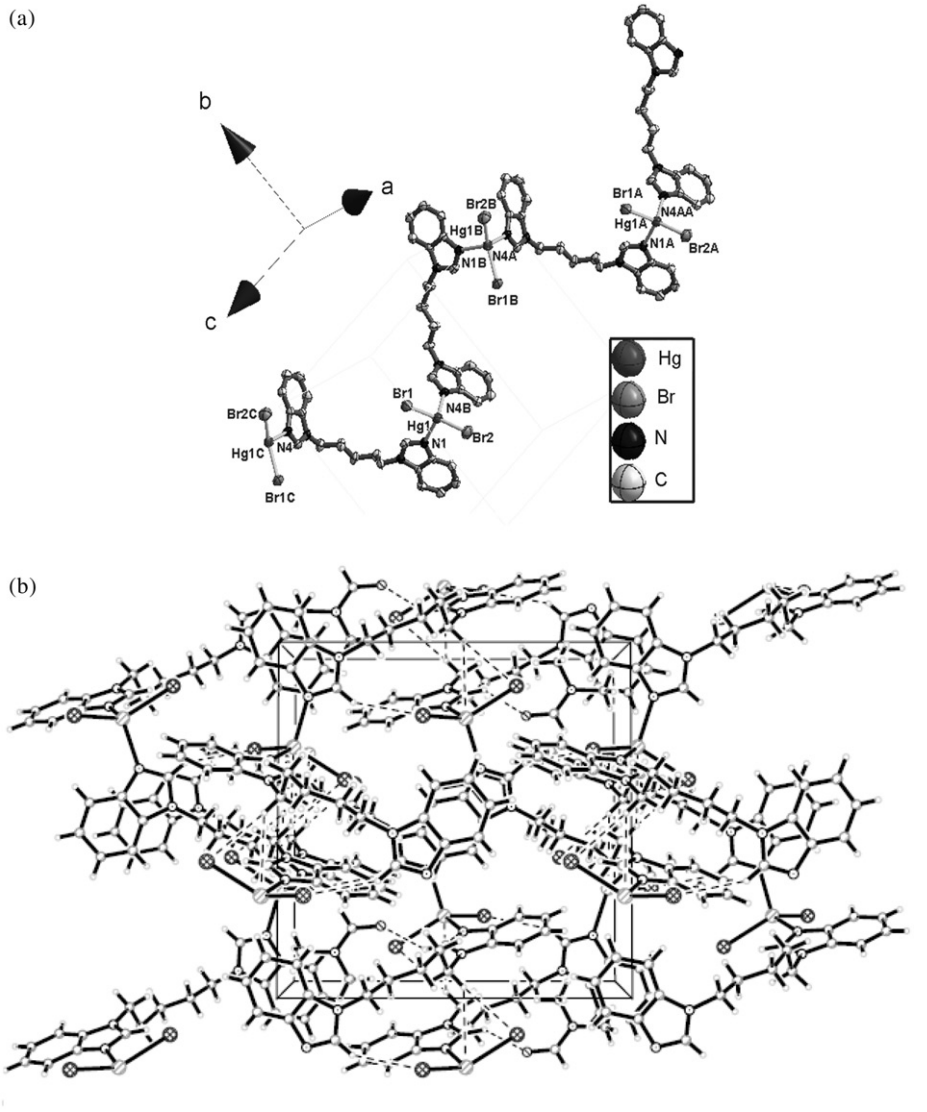

Figure 1. (a) View of the 1-D zigzag chain showing local coordination environment of Hg^{2+} ions (50% thermal ellipsoids); all hydrogen atoms are omitted for clarity. (b) View of the 3-D network for **1** viewed along the *a*-axis.

In addition, hydrogen-bonding interactions exist in **1**, constructed by free DMF molecules (O1). The structure of **1** also contains numerous inter-chain C–H $\cdots\pi$ supramolecular interactions between phenyl and imidazole rings of pbbm ligands to generate a 3-D supramolecular framework (figure 1b).

3.2. *Crystal structure of* $[HgI_2(pbbm)]_2$ *(2)*

To explore the effect of the counteranion on the topology of the resultant network, the reaction of pbbm with HgI_2 is performed to give **2**. Crystallographic analysis provides

direct evidence that the structure of **2** is different from that of **1**. Complex **2** consists of a centrosymmetric wheel-shaped dinuclear neutral molecule $[HgI_2(pbbm)]_2$ (figure 2a). In the dinuclear unit, there are two crystallographically identical Hg(II) centers bridged by two pbbm ligands. Each Hg(II) center is coordinated by two nitrogen atoms from different pbbm ligands and two terminal iodine atoms to form a distorted $[HgN_2I_2]$ tetrahedron. The Hg–N bond lengths of 2.302(6) and 2.418(7) Å are different from those observed in **1**, and those of Hg–I are 2.6513(7) and 2.7156(7) Å, which are similar to those of the related complexes $[HgI_2(L)]_n$ (Hg–I ranging from 2.6430(5) to 2.6683(8) Å and Hg–N from 2.3626(6) to 2.457(6) Å) [16], and are all within normal values. The bond angles of N–Hg–I are from 98.46(16)° to 115.86(15)° and I–Hg–I is 131.12(2)°. In the solid structure of **2**, binuclear units are linked through hydrogen bonds and inter-chain C–H $\cdots\pi$ supramolecular interactions, generating a 3-D supramolecular structure as shown in figure 2(b).

In summary, **1** and **2** contain the same pbbm and Hg(II) centers with identically tetrahedral configuration, but the discrete binuclear structure of **2** is a striking contrast to the 1-D zigzag chain of **1**. This may be explained by the different sizes of Br^- and I^- and demonstrate the significant effect of counteranion on the assembly and topology of the resultant MOFs. Complex **1** assumes the same structure as our previous report $\{[Cu(Ac)_2(pbbm)]\cdot CH_3OH\}_n$ despite having a different counteranion Ac^- and different central metal Cu [10], which indicates that the ligand geometry takes an essential role in framework formation of complexes. As a result, it seems that the selection of appropriate flexible ligand, central metal, and counteranion would be an ideal way to construct MOFs.

3.3. *XRPD results*

To confirm whether the crystal structure is truly representative of the bulk materials for related ion-exchange measurements of **1** and **2**, XRPD experiments have been carried out for **1** and **2**. The XRPD experimental and computer-simulated patterns of the corresponding complexes are shown in figure 3. Although the experimental patterns have few unindexed diffraction lines and some are slightly broadened in comparison with those simulated from the single-crystal models, it can still be considered that the bulk synthesized materials and the as-grown crystals are homogeneous for **1** and **2**.

3.4. *Ion-exchange behavior*

Stable porous coordination networks have been reported to serve as ion exchangers because they exhibit analogous structures with zeolites [17]. It is important, thus, to evaluate the ion-exchange properties of coordination networks for potential applications. In an initial test for anion exchange, some freshly prepared crystals of **1** were soaked in an aqueous solution of KI (0.3 mmol) and left undisturbed at room temperature. After *ca* 6 days, the products were filtered off, washed several times with water, and then dried in air. The final ion-exchanged products (**1**-I) of **1** were identified by IR spectra, SEM, EDS, and XRPD. Analogous IR spectra of **1** and its ion-exchanged product **1**-I verified that the coordination polymer retained its structure (figure 4). From XRPD patterns (figure 3a), it is obvious that the main peaks of **1** were also kept in patterns of **1**-I. Meanwhile, the exchange of I^- ions produced several new

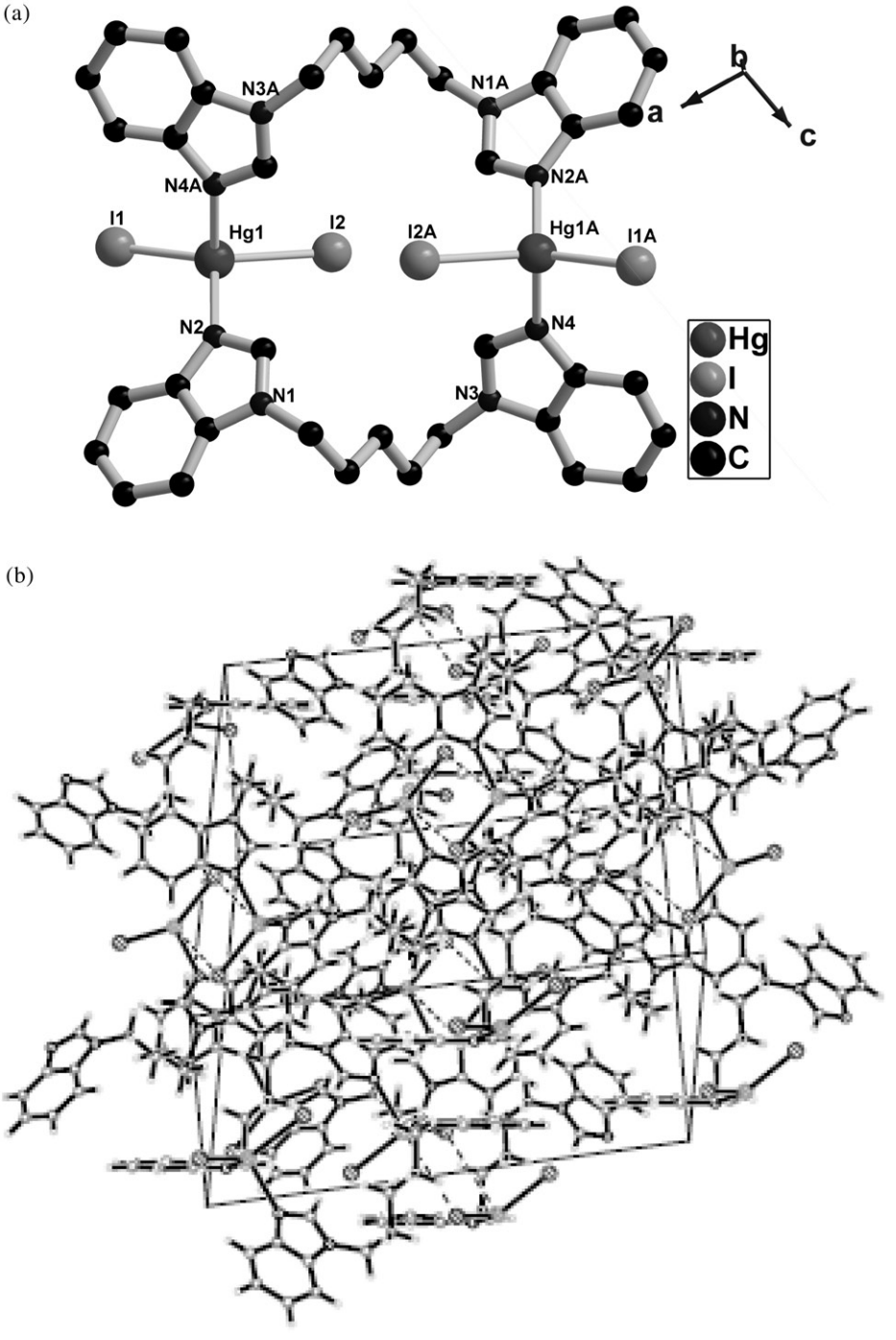

Figure 2. (a) View of the binuclear structure of **2**. (b) View of the infinite 3-D supramolecular structure of **2**, generated through extensive hydrogen-bonding and C–H $\cdots\pi$ interactions.

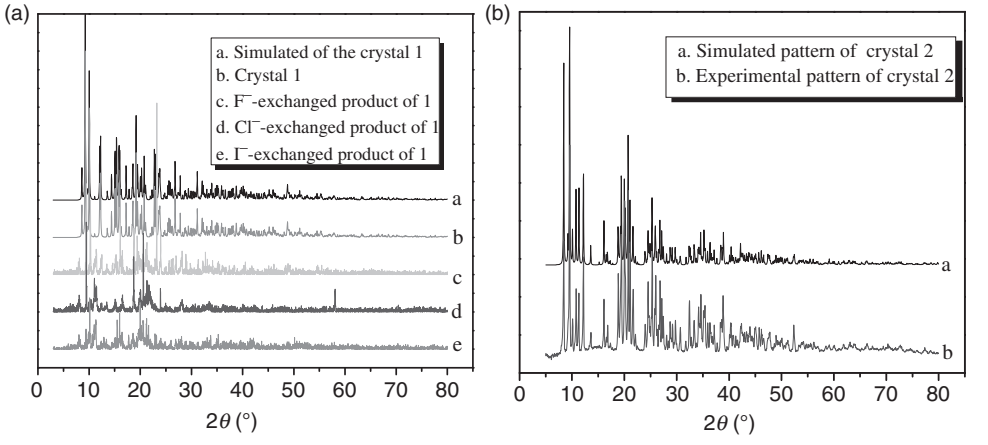

Figure 3. (a) XRPD patterns of **1** and its F^-, Cl^-, and I^--exchanged products (a, b represent XRPD computer-simulated patterns and experimental of **1**, respectively; c, d, e represent XRPD patterns of its F^-, Cl^-, and I^--exchanged products, respectively). (b) XRPD patterns of **2** (a, b represent XRPD computer-simulated patterns and experimental of **2**, respectively).

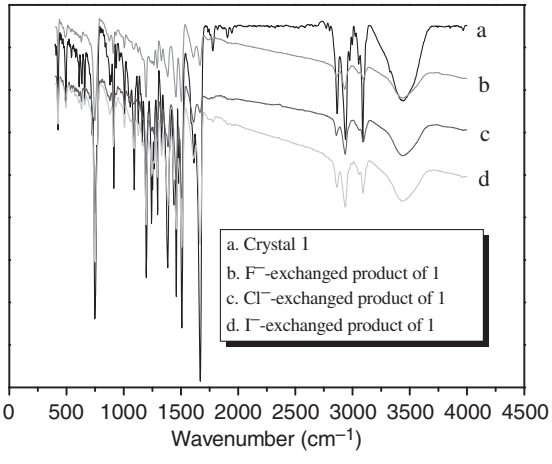

Figure 4. IR spectra of **1** and its F^-, Cl^-, and I^--exchanged products (a represents IR patterns of **1**; b, c, d represent IR patterns of its F^-, Cl^-, and I^--exchanged products, respectively).

peaks and also made the main peaks of **1** shift a bit. The EDS revealed that there was a higher I^- content (figure 5), indicating that the metathesis reaction took place and the Br^- ions of **1** were partially exchanged with I^-.

The anion-exchange behavior in **1** shows that this kind of complex has strong exchange ability to I^-. In the interest of clarifying this behavior, several influences including the amount of **1**, the soak time as well as the concentration of KI solution are studied. Figure 6 depicts the effect of the amount of **1** on the exchanged percentages of Br^-. It is apparent that the continuously improved percentage of exchanged Br^- is obtained at low amounts of **1**, whereas at higher amounts of **1**, the percentage of

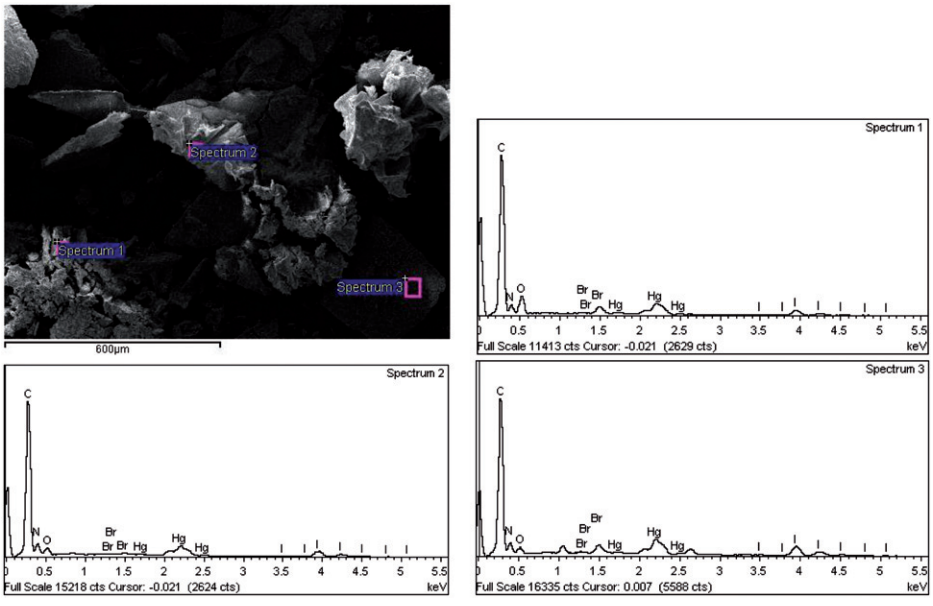

Figure 5. SEM and EDS of the I^--exchanged product for **1** after trituration.

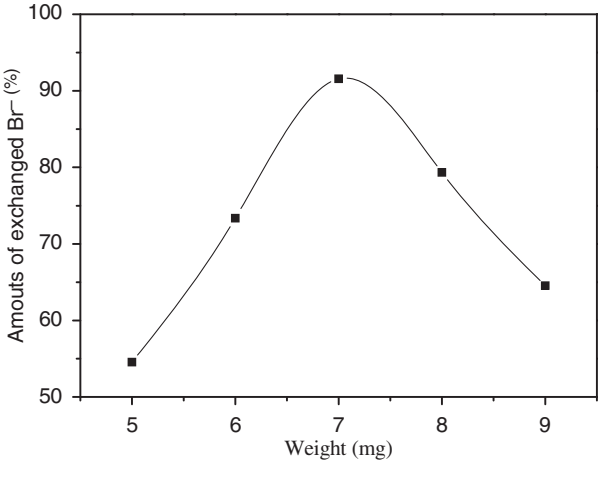

Figure 6. The percentage of exchanged Br^- with different masses of crystalline **1**.

exchanged Br^- decreases. The optimum amount of **1** is found to be 7 mg. The effect of soak time on the percentages of exchanged Br^- is illustrated in figure 7, showing the percentage of exchanged Br^- gradually rising along with the increase in soak time for 8 days, reaching a value of 100%. The influence of the concentration of KI solution is studied by using 0.1, 0.2, 0.3, 0.4, 0.5, 0.6 mg mL^{-1} (figure 8). Clearly, the percentage of exchanged Br^- increases as the concentration of KI solution increases. A steady state of

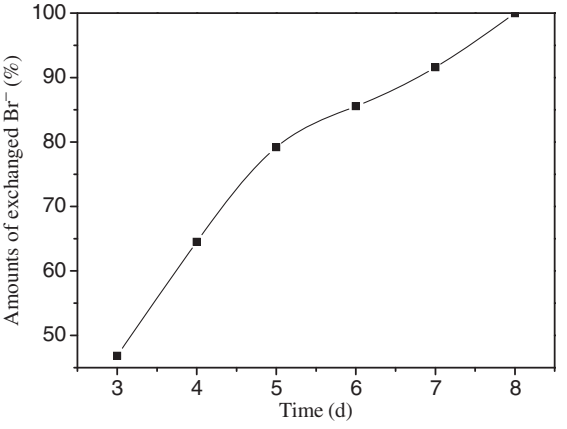

Figure 7. The effect of soak time on the percentages of exchanged Br^-.

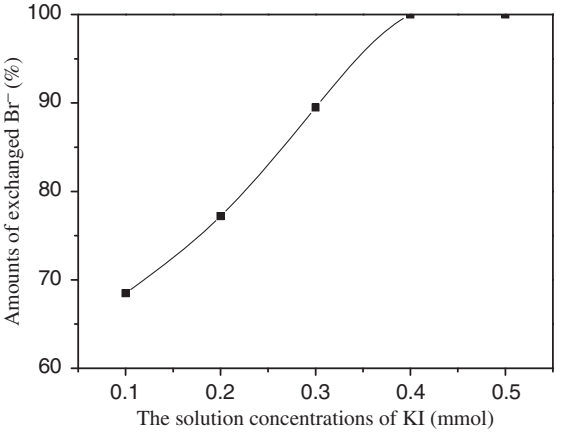

Figure 8. The percentage of exchanged Br^- of crystalline **1** in different solution concentrations of KI.

the metathesis reaction is observed in 0.4 mmol L^{-1} KI solution. Further increase in the concentration of KI solution cannot improve the percentage of exchanged bromide significantly, which indicates that the percentage of exchanged bromide would be finite.

Anion-exchange properties of organic–inorganic hybrid materials are closely associated with the anions' electronegative ability and the coordination ability of metal ions to anion [18]. Hence, we assess ion-exchange capacity of crystalline **1** toward F^-, Cl^-, and I^- under the optimized reaction conditions by using a JSM 6490LV electron microscope. As shown in figures 3 and 4, analogous XRPD analysis and IR spectra verify that the exchanged products retain the structure of **1**. The EDS data reveal that anion exchange of **1** was highly selective; only substitution of Br^- by I^- was achieved, whereas attempted anion exchange of Br^- by F^-, and Cl^- were unsuccessful. In similar experiments, **2** remained in its crystalline form and EDS analysis indicated that **2** could not undergo ion exchange, whether it was immersed for 8 or 30 days.

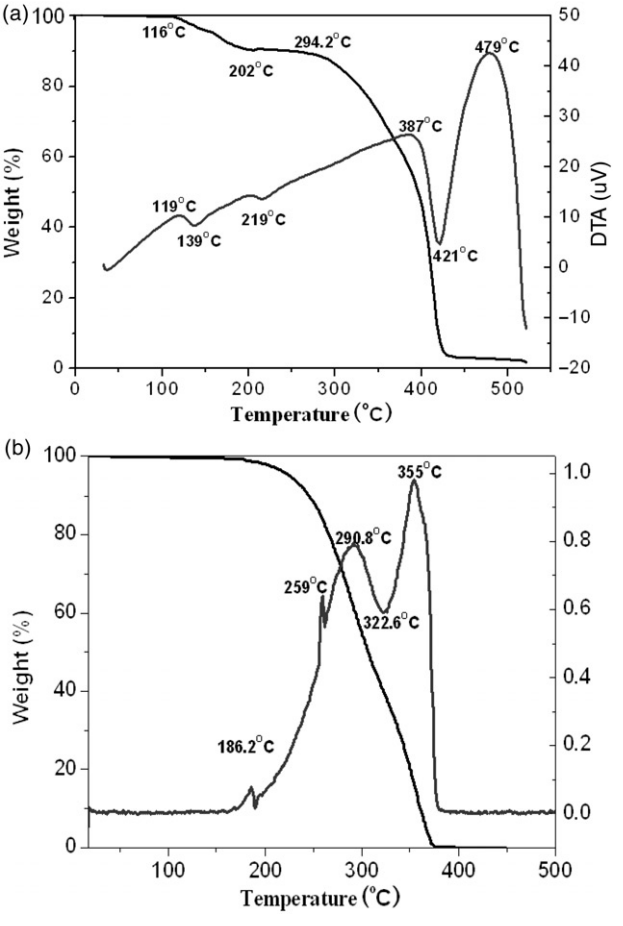

Figure 9. TG-DTA curve for **1** and **2** (a, b represent **1** and **2**, respectively).

We presume that this could be attributed to steric hindrance, the ionic radius and the difference in coordination abilities of the ingoing anions to central Hg^{2+} ions.

3.5. *TGA of complexes*

To examine thermal stabilities of the coordination architectures, TGA of the crystalline material was performed. The TGA curves of the two complexes indicate that the framework of **1** begins to collapse from 116°C, and **2** is stable to 191°C, where the decomposition of the framework starts. For **1** (figure 9a), the weight loss of 9.63% from 116°C to 202°C corresponds to removal of free DMF (theoretical: 9.91%), then keeps losing weight from 294.2°C to 425°C corresponding to removal of the organic species. One weak endothermic peak (119°C), two weak exothermic peaks (139°C and 219°C), two strong endothermic peaks (387°C and 479°C), and one strong exothermic peak (421°C) in the DTA curve correspond to weight loss of various groups. For **2**, the rapid

weight loss from 185°C to 376°C corresponds to removal of the corresponding organic components and HgI_2. There are two weak endothermic peaks (186°C and 259°C), two strong endothermic peaks (291°C and 355°C), and one very strong exothermic peak (323°C) on the DTA curve of **2**.

4. Conclusion

We have synthesized and structurally characterized two Hg(II)-containing adducts through rational self-assembly. The anion-exchange behavior was investigated, suggesting that coordinated anion exchange can take place in metal–organic coordination architectures. This result has significance to provide a useful channel in exploration of new solid state ion-exchange materials.

Supplementary material

CCDC 808788 and 841972 contain the supplementary crystallographic data for **1** and **2**, respectively. These data can be obtained free of charge from the Cambridge Crystallographic Data Centre *via* www.ccdc.cam.ac.uk/data_request/cif. Supplementary data associated with this article can be found, in the online version, at doi:10.1016/j.ica.2011.04.008.

Acknowledgments

This work was supported by A Project Funded by the Priority Academic Program Development of Jiangsu Higher Education Institutions (PAPD).

References

[1] S. Kitagawa, R. Kitaura, S.I. Noro. *Angew. Chem., Int. Ed.*, **43**, 2334 (2004).
[2] S.M. Humphrey, P.T. Wood. *J. Am. Chem. Soc.*, **126**, 13236 (2004).
[3] D.G. Mantero, A. Neels, H. Stoeckli-Evans. *Inorg. Chem.*, **45**, 3287 (2006).
[4] H.K. Liu, X.H. Huang, T.H. Lu, X.J. Wang, W.Y. Sun, B.S. Kang. *Dalton Trans.*, 3178 (2008).
[5] B.C. Tzeng, T.H. Chiu, B.S. Chen, G.H. Lee. *Chem. Eur. J.*, **14**, 5237 (2008).
[6] Y.C. Qiu, Z.H. Liu, Y.H. Li, H. Deng, R.H. Zeng, M. Zeller. *Inorg. Chem.*, **47**, 5122 (2008).
[7] P. Wang, A. Anderko, D.R. Turner. *Ind. Eng. Chem. Res.*, **40**, 4444 (2001).
[8] H.J. Choi, M.P. Suh. *Inorg. Chem.*, **42**, 1151 (2003).
[9] Y. Wang, P. Cheng, Y. Song, D.Z. Liao, S.P. Yan. *Chem. Eur. J.*, **13**, 8131 (2007).
[10] X.R. Meng, B. Xiao, Y.T. Fan, H.W. Hou, G. Li. *Inorg. Chim. Acta*, **357**, 1471 (2004).
[11] A.X.S. Bruker. *SAINT Software Reference Manual*, Madison, WI (1998).
[12] G.M. Sheldrick. *SADABS, Siemens Area Detector Absorption Corrected Software*, University of Göttingen, Germany (1996).
[13] G.M. Sheldrick. *SHELXTL NT, Version 5.1; Program for Solution and Refinement of Crystal Structures*, University of Göttingen, Germany (1997).

[14] Y.Y. Niu, H.W. Hou, Y.L. Wei, Y.T. Fan, Y. Zhu, C.X. Du, X.Q. Xin. *Inorg. Chem. Commun.*, **4**, 358 (2001).
[15] Y.Y. Niu, Y.L. Song, H.W. Hou, Y. Zhu. *Inorg. Chim. Acta*, **355**, 151 (2003).
[16] (a) H.W. Hou, L.K. Li, G. Li, Y.T. Fan, Y. Zhu. *Inorg. Chem.*, **42**, 3501 (2003); (b) Y.Y. Niu, Y.L. Song, J. Wu, H.W. Hou, Y. Zhu, X. Wang. *Inorg. Chem. Commun.*, **7**, 471 (2004); (c) Y.Y. Niu, N. Zhang, Y.L. Song, H.W. Hou, Y.T. Fan, Y. Zhu. *Inorg. Chem. Commun.*, **8**, 495 (2005).
[17] A.L. Spek. *PLATON, A Multipurpose Crystallographic Tool*, Utrecht University, Utrecht, The Netherlands (2005).
[18] H.Y. Yang, L.K. Li, J. Wu, H.W. Hou, B. Xiao, Y.T. Fan. *Chem. Eur. J.*, **15**, 4045 (2009).